
AFRL-RX-WP-TP-2011-4068

# DEPLETION-INDUCED SHAPE AND SIZE SELECTION OF GOLD NANOPARTICLES (POSTPRINT)

**Kyoungweon Park, Hilmar Koerner, and Richard A. Vaia**

**Nanostructured and Biological Materials Branch**
**Nonmetallic Materials Division**

**JANUARY 2011**



**AIR FORCE RESEARCH LABORATORY**
**MATERIALS AND MANUFACTURING DIRECTORATE**
**WRIGHT-PATTERSON AIR FORCE BASE, OH 45433-7750**
**AIR FORCE MATERIEL COMMAND**
**UNITED STATES AIR FORCE**

# REPORT DOCUMENTATION PAGE

*Form Approved*
*OMB No. 0704-0188*



| 1. REPORT DATE *(DD-MM-YY)* | 2. REPORT TYPE | 3. DATES COVERED *(From - To)* |
|---|---|---|
| January 2011 | Journal Article Postprint | 01 January 2009 – 03 January 2011 |

**4. TITLE AND SUBTITLE**
DEPLETION-INDUCED SHAPE AND SIZE SELECTION OF GOLD NANOPARTICLES (POSTPRINT)

**5a. CONTRACT NUMBER**
In-house

**5b. GRANT NUMBER**

**5c. PROGRAM ELEMENT NUMBER**
61102F

**6. AUTHOR(S)**
Kyoungweon Park, Hilmar Koerner, and Richard A. Vaia

**5d. PROJECT NUMBER**
2303

**5e. TASK NUMBER**
C0

**5f. WORK UNIT NUMBER**
BN123100

**7. PERFORMING ORGANIZATION NAME(S) AND ADDRESS(ES)**

Nanostructured and Biological Materials Branch (AFRL/RXBN)
Nonmetallic Materials Division
Materials and Manufacturing Directorate
Wright-Patterson Air Force Base, OH 45433-7750
Air Force Materiel Command, United States Air Force

**8. PERFORMING ORGANIZATION REPORT NUMBER**
AFRL-RX-WP-TP-2011-4068

**9. SPONSORING/MONITORING AGENCY NAME(S) AND ADDRESS(ES)**
Air Force Research Laboratory
Materials and Manufacturing Directorate
Wright-Patterson Air Force Base, OH 45433-7750
Air Force Materiel Command
United States Air Force

**10. SPONSORING/MONITORING AGENCY ACRONYM(S)**
AFRL/RXBN

**11. SPONSORING/MONITORING AGENCY REPORT NUMBER(S)**
AFRL-RX-WP-TP-2011-4068

**12. DISTRIBUTION/AVAILABILITY STATEMENT**
Approved for public release; distribution unlimited.

**13. SUPPLEMENTARY NOTES**
Journal article published in ACS *NANO Letters*, Vol.10, March 29, 2010, p. 1433-1439.

 Technical paper contains color.

PAO Case Number and clearance date: 88ABW-2010-6407, 06 Dec 2010.

**14. ABSTRACT**
For nanoparticle-based technologies, efficient and rapid approaches that yield particles of high purity with a specific shape and size are critical to optimize the nanostructure-dependent optical, electrical, and magnetic properties, and not bias conclusions due to the existence of impurities. Notwithstanding the continual improvement of chemical methods for shaped nanoparticle synthesis, byproducts are inevitable. Separation of these impurities may be achieved, albeit inefficiently, through repeated centrifugation steps only when the sedimentation coefficient of the species shows sufficient contrast. We demonstrate a robust and efficient procedure.

**15. SUBJECT TERMS**
metamaterials, nanoparticles

| 16. SECURITY CLASSIFICATION OF: | | | 17. LIMITATION OF ABSTRACT: | 18. NUMBER OF PAGES | 19a. NAME OF RESPONSIBLE PERSON (Monitor) |
|---|---|---|---|---|---|
| a. REPORT | b. ABSTRACT | c. THIS PAGE | | | Katie Thorp |
| Unclassified | Unclassified | Unclassified | SAR | 12 | 19b. TELEPHONE NUMBER *(Include Area Code)* N/A |

**Standard Form 298 (Rev. 8-98)**
Prescribed by ANSI Std. Z39-18

NANO LETTERS

pubs.acs.org/NanoLett

# Depletion-Induced Shape and Size Selection of Gold Nanoparticles

**Kyoungweon Park, Hilmar Koerner, and Richard A. Vaia***

Materials and Manufacturing Directorate, Air Force Research Laboratory, Wright-Patterson AFB, Ohio 45433-7702

**ABSTRACT** For nanoparticle-based technologies, efficient and rapid approaches that yield particles of high purity with a specific shape and size are critical to optimize the nanostructure-dependent optical, electrical, and magnetic properties, and not bias conclusions due to the existence of impurities. Notwithstanding the continual improvement of chemical methods for shaped nanoparticle synthesis, byproducts are inevitable. Separation of these impurities may be achieved, albeit inefficiently, through repeated centrifugation steps only when the sedimentation coefficient of the species shows sufficient contrast. We demonstrate a robust and efficient procedure of shape and size selection of Au nanoparticles (NPs) through the formation of reversible flocculates by surfactant micelle induced depletion interaction. Au NP flocculates form at a critical surfactant micelle molar concentration, $C_m$* where the number of surfactant micelles is sufficient to induce an attractive potential energy between the Au NPs. Since the magnitude of this potential depends on the interparticle contact area of Au NPs, separation is achieved even for the NPs of the same mass with different shape by tuning the surfactant concentration and extracting flocculates from the sediment by centrifugation or gravitational sedimentation. The refined NPs are redispersed by subsequently decreasing the surfactant concentration to reduce the effective attractive potential. These concepts provide a robust method to improve the quality of large scale synthetic approaches of a diverse array of NPs, as well as fine-tune interparticle interactions for directed assembly, both crucial challenges to the continual realization of the broad technological potential of monodispersed NPs.

**KEYWORDS** Shape separation, gold nanorods, depletion interaction, scale-up purification, nanoparticles

The physical and chemical properties of nanoparticles (NPs) are determined and limited by the distribution of their physical dimensions and shape.[1] Numerous innovations, focusing on independent, sequential control of nucleation, growth, coarsening, and final product etching, now provide an incredible array of complex structures.[2−5] This control however requires precise process management of environmental conditions (i.e., prescribed history of uniformity, rate, and gradients of temperature and concentration) that in many instances are not necessarily amenable to large scale NP synthesis. Thus, undesired size and shape impurities still occur at unacceptable levels, especially for the metal NPs synthesized by wet chemical methods[6] and via large scale synthesis methodologies.[7] In these instances, refined NP distribution is still needed to better challenge theoretical concepts and models.[8] Therefore, development of efficient and rapid approaches to separate a specific shape or size from an ensemble mixture is critical for general nanoparticle fabrication.

As a focused system, consider Au nanorods (NRs), which have garnered substantial interest for various technologies including optical filtering, subwavelength imaging, data storage, and sensor devices.[9,10] The most efficient approach in preparing large quantities of Au NRs is via seed-mediated synthesis in the presence of a surfactant.[11] For many optical applications though, the polydispersity in rod size and byproducts in the form of nanospheres and nanoplates limit full utilization. Depending on synthesis conditions, the fraction of byproducts can range from 10%, to almost 90%.[11,12] To separate the desired NRs, capillary electrophoresis[13] and column chromatography[14] have been explored. But yield, resolution, and throughput of the separation are limited. On the other hand, centrifugation is a common part of the procedure used to separate excess surfactant from the reaction medium as well as to concentrate the NP samples. It can also provide crude separation. For example, spherical particles larger than ~60 nm can be removed by collecting the sedimentation at lower centrifugation speeds (~3000 rpm).[12] Smaller size spheres (<~5 nm) can be separated as supernatant through repeated centrifugation at higher speed (6000−14500 rpm).[15] For example, Khanal et al.[16] reported the separation of smaller Au spherical particles from rods and platelets and attributed the separation to the different mass-dependent sedimentation coefficient of the NPs. They further separated platelets from rods after the oxidation of the gold nanostructures, which reduced the size of the platelets more effectively than that of the rods. Recently, Sharma et al. elucidated the hydrodynamic behavior of Au NPs of various shapes to identify the parameters necessary to achieve efficient separation.[17] They found that shape-dependent drag causes particles to have a shape-dependent sedimentation behavior in addition to that of mass. In these cases however, the ability to fine-tune the separation, especially at larger scale and between rods of slightly different length, is difficult.

* To whom correspondence should be addressed, richard.vaia@wpafb.af.mil.
**Received for review:** 01/29/2010
**Published on Web:** 03/29/2010

**SCHEME 1. Depletion-Induced Flocculation of Larger Nanoparticles for Separation of Multicomponent Colloidal Solutions.** [a]

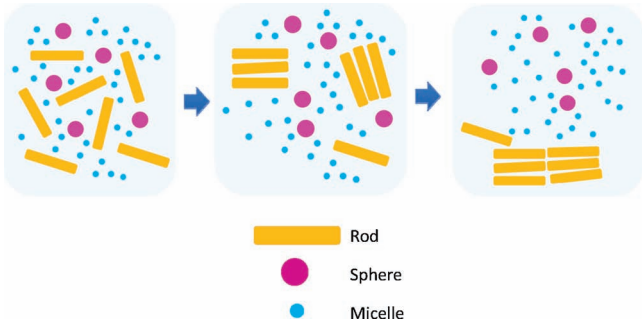


[a] Small and numerous micelles create an entropic, short-ranged depletion attraction between the largest NPs. This results in preferential aggregation and sedimentation, leaving relatively smaller NPs in the solution (not to scale).

Scheme 1 summarizes a separation methodology using an effective depletion interaction between NPs induced by the surfactant micelles present in the reaction mixture. Shape and size selection of Au NPs can be achieved by tuning the surfactant micelle concentration to create an entropic, short-ranged depletion attraction between Au NPs. This results in preferential aggregation and sedimentation of one species, leaving the other species in the solution.

Depletion interactions between colloidal particles arise when the separation distance between colloids is on the order of the size of a smaller, more abundant second component. The exclusion of this component from the space between the colloids results in a local concentration gradient that produces an attractive osmotic pressure. Asakura and Oosawa (AO)[18] were one of the first to systematically demonstrate that an effective attraction between colloids arises from the addition of a free polymer or surfactant above a critical concentration. This depletion-induced phase separation has been demonstrated in various systems.[19−21] However, the utilization of depletion induced phase separation to isolate one species from others has only been tentatively demonstrated with limited precision for carbon nanotubes[22] and viruses.[23] Therefore, the feasibility and limitation of the systematic application of depletion induced phase separation to isolate a desired size and shape of NPs from a multicomponent mixture is unknown.

The potential energy, $U$, rising from the depletion of micelles between two particles at contact can be estimated via the AO model[18] as the product of the excluded volume, $V_e$, and the micellar osmotic pressure, $\Pi_m$

$$U = -V_e\Pi_m$$

where the negative sign indicates a favorable (attractive) change in the particle pair potential. $V_e$ is determined by the shape and size of the NP and surfactant micelle. $\Pi_m$ is $C_mN_0k_BT$ where $k_B$ is Boltzmann's constant, $N_0$ is Avogadro's number, $C_m = (c - c^*)/n$ is the micelle molar concentration, $c$ is the molar concentration of surfactant, $c^*$ is critical micelle concentration, and $n$ is the number of surfactant molecules to form a micelle (aggregation number).[20] $|U|$ between two particles can be increased (or decreased) by increasing (or decreasing) the number of micelles, $C_m$.

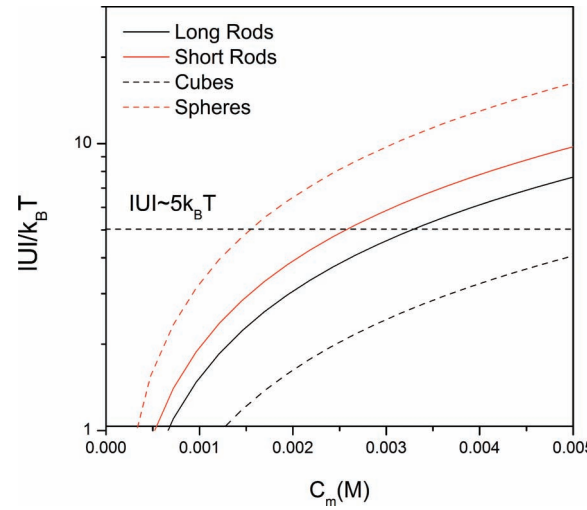


**FIGURE 1. The depletion interaction potential, $|U|/k_BT$, as a function of micelle molar concentration, $C_m$, based on the AO model for NPs obtained in typical seed-mediated Au NR synthesis method: long rod, 77 nm in length and 11 nm in diameter; short rod, 60 nm in length and 18 nm in diameter; cube, 15 nm in edge length; sphere, 60 nm in diameter.**

For example, Figure 1 summarizes the depletion potential between typical Au NRs and their impurities (large polycrystalline spheres and cubes) as a function of the molar concentration of surfactant micelle. The depletion potential was calculated based on the side-by-side arrangement which gives rise to maximum interaction potential.

$$U = -(2a_m)Ld'\Pi_m$$

$a_m$ is radius of the surfactant micelle which was assumed as 3 nm, consistent with experimental observations.[24,25] The shape of the rod was approximated as a parallelepiped with two flat ends and prismatic sides ($L$ is length of rod and $d$ is width of rod), consistent with reported crystallography.[26] Therefore, the excluded volume can be estimated by the product of the rod's prismatic side area ($L \times d'$,$d'$ is effective edge length) with the micelle diameter. $d'$ can range from $0.41d$(octagonal prism) to $d$(rectangular prism). $d'$ was assumed as $0.5d$ in this calculation based on the most frequently observed structure of rods by transmission electron microscopy (TEM) observation. The shape of the polycrystalline sphere was approximated as cuboctahedron based on TEM observation and excluded volume between the spheres and that between cubes were approximated as $2a_m \times d'^2$.



DOI: 10.1021/nl100345u | *Nano Lett.* **2010,** *10,* 1433--1439

In general, as micelle concentration increases, the attractive pairwise potential between colloids increases, but in a manner that depends on their topology. Colloidal flocculation generally occurs if the potential exceeds $\sim 4-5k_BT$[27,28](defined as critical potential: $|U_c|$). Thus, a critical micelle molar concentration to form aggregates, $C_m$* can be defined when $|U(C_m^*)| \sim |U_c|$. Accordingly, a concentration range of surfactant exists in which the attractive potential between one species will favor flocculates, whereas the other will remain stable in solution. Since the sedimentation coefficient of the flocculates is proportional to the number of NPs within the flocculate, the difference in effective sedimentation rates between NP species increases, allowing easier gravitational (or low speed centrifugal) separation. Therefore, by knowing $C_m$* for each NP in a given surfactant system, one can separate one species of particles from the other by adjusting the surfactant concentration assuming that the surfactant micelle is smaller and more numerous than the various NPs in solution. Finally, since the depletion interaction depends on $C_m$, the NPs can be subsequently redispersed from the flocculates by decreasing the surfactant concentration.

As an example, consider a typical synthesis of Au NRs with CTAB/BDAC binary surfactants as stabilizer. Here, relatively long NRs ($L/d \sim 7$ with $d \sim 11$ nm) can be obtained with nanocube (edge length ~20 nm) impurity.[29] At a surfactant concentration of 0.225 M (0.1 M of CTAB and 0.125 M of BDAC) and a NP concentration of 0.1 nM, a thin film of dark color forms at the bottom of the solution flask after 24 h. This sediment is redispersible after decanting the supernatant by decreasing surfactant concentration through addition of Milli Q water to the flask. Panels a−c of Figure 2 summarize the particles contained in as-made solution, the rod-rich sediment, and cube-rich supernatant, respectively, and qualitatively demonstrates the separation of rods from the impurity. Here, the surfactant concentration (0.225 M) corresponds to a micelle molar concentration of ~3.6 mM, $10^7$ times greater than Au rod concentration. Micelle molar concentration, $C_m$ is calculated according to the aforementioned equation, $C_m = (c - c^*)/n$. For a CTAB/BDAC mixture, BDAC dominates overall properties over most of the mole fraction range.[30] Therefore $c^*$ and $n$ of BDAC (0.0005 M[30] and 62,[31] respectively) were used for the calculation. Furthermore, the stabilizing surfactant bilayer surrounding each NP only accounts for approximately 0.005% of the total surfactant concentration; thus the vast majority of surfactant molecules are associated with micelles. From the AO model, $|U|$ between rods is $\sim 5.5k_BT$ while that between the cubes is $\sim 2.9k_BT$, consistent with the experimentally observed rod-rich flocculates.

Alternatively, consider Au NR synthesis with CTAB as a stabilizer (0.1 M). A stable colloidal dispersion of relatively short NRs ($L/d \sim 2.9$, $d = 18$ nm) are obtained with large polycrystalline particles ($d = 60$ nm).[32] At this initial CTAB concentration (corresponding $C_m$ is 0.6 mM, which is calculated assuming that $c^*$ and $n$ of CTAB are 0.001M[30] and 163,[24,33] respectively), $|U|$ between rods is $\sim 1.2k_BT$ and that between the spherical impurities is $\sim 2.0k_BT$, consistent with the absence of flocculates. At CTAB concentration of 0.25 M (corresponding $C_m$ is 1.5 mM), calculated $|U|$ between rods is $\sim 2.9k_BT$ and that between spheres is $\sim 4.9k_BT$, implying only spheres should form flocculates. Indeed, increasing the surfactant concentration to 0.25 M with additional CTAB results in sediment after 24 h that is comprised of flocculates of the large polycrystalline spherical particles. These were also subsequently redispersible upon addition of Milli Q water. Panels d−f of Figure 2 summarize the particles contained in the as-made, sphere-rich sediment, and rod-rich supernatant, respectively.

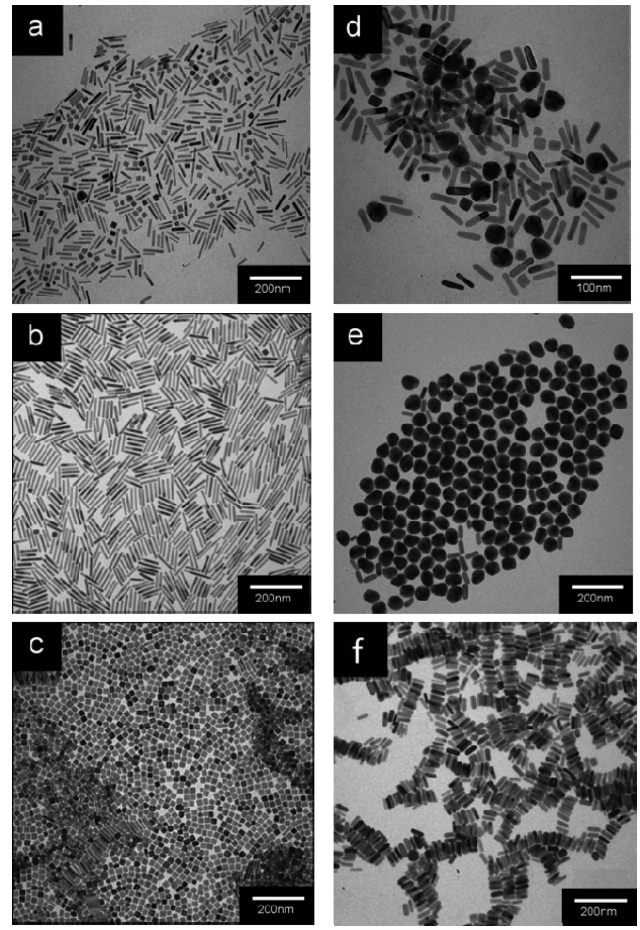


**FIGURE 2. TEM images of Au nanorod products before and after separation: CTAB/BDAC method,[11] (a) As-made NR product, (b) sediment containing NRs ($L = 77$ nm, $d = 11$ nm), and (c) supernatant containing cubes ($L = 20$ nm); CTAB method,[11] (d) As-made NR product, (e) sediment containing large polycrystalline spheres ($d = 60$ nm), and (f) supernatant containing rods ($L = 60$ nm, $d = 18$ nm).**

In both cases, summarized in Figure 2, the number fraction of rods increased from 77% and 73% for the crude long and short NR products, respectively, to ~99.9% for the separated products after only one sedimentation−



DOI: 10.1021/nl100345u | *Nano Lett.* **2010,** *10,* 1433--1439

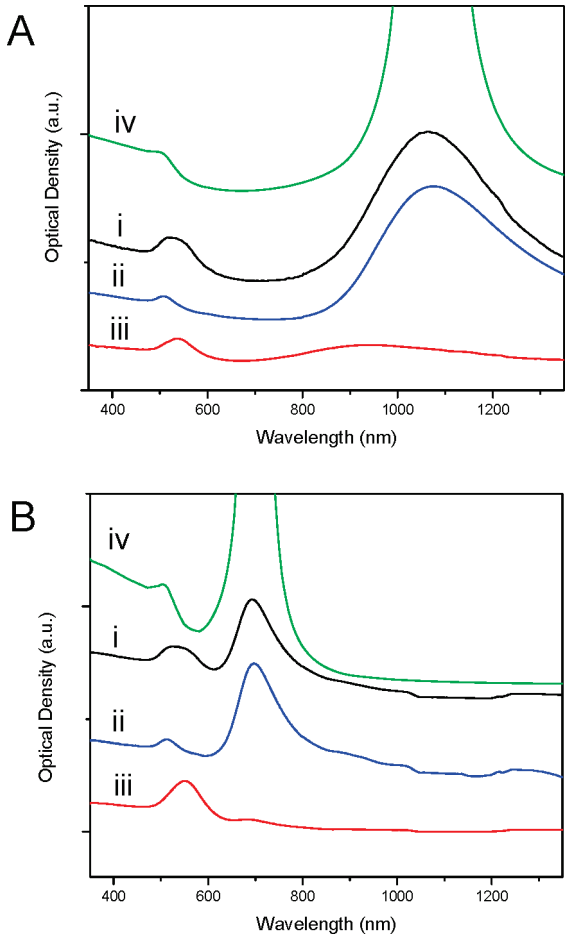


**FIGURE 3. Normalized UV−vis−NIR spectra of crude and separated products from CTAB/BDAC synthesis of long Au NRs ($L/d = 7$) (A) and CTAB synthesis of short Au NRs ($L/d = 3$) (B) summarized in Figure 2. Black (i), as made; blue (ii), separated rods; red (iii), separated impurities; and green (iv), the extinction spectrum calculated with the expressions of Gans for elongated ellipsoids using the bulk optical data for gold.[34] Purified Au NR solutions exhibit resonances that are narrower and more consistent with theoretical predictions.**

redispersion cycle. Additionally, 80% of synthesized NRs were collected through the separation procedure, leaving only 20% of rods with the impurity.

By reducing the number density of shape impurities, the agreement between theoretical prediction and the measured breadth and peak position of the transverse plasmon resonances improves.[34] Figure 3 summarizes UV−vis−NIR spectra of the particle solutions before and after separation. The spectra were taken after redispersing the particles in Milli Q water. For as-made solution, the longitudinal peak is consistent with prediction. But the transverse peak (around 530 nm) is broad due to the impurities. Upon separation, the transverse peak becomes smaller and narrower appearing at around 505 nm, which is consistent with the prediction.[2]

It is important to note that not only does the number density of micelles depend on the concentration of surfactant above $c^*$, but so does shape. With increasing concentration, spherical surfactant micelles coalesce into rodlike, and ultimately wormlike micelles.[35] Experimentally, the surfactant concentration for these transitions depends on electrolyte concentration, temperature, and pH. These larger structures, and associated reduced number density, will not result in as strong of depletion interactions between nanoparticles and, thereby, establish an upper limit of particle surfactant concentration. Empirically, we found for the aforementioned reactions, a CTAB solution of ~0.3 M becomes visibly viscoelastic suggesting the formation of entangled wormlike micelles. This is consistent with prior reports.[33] This transition increases at elevated temperatures, suggesting some latitude in processability. Alternatively, CTAB/BDAC mixtures exhibit a rapid viscosity increase, indicative of the transition to wormlike micelles, at a much higher concentration (>0.5 M). Also, BDAC forms micelles at a lower critical concentration, $c^*$, than CTAB ($c^*$(BDAC), 0. 0005 M; $c^*$(CTAB) 0.001 M),[30] with a smaller number per micelle (62 for BDAC at 0.1 M,[31] 163 for CTAB at 0.1 M[24,33]). The result is a larger micelle molar concentration, $C_m$, and thus greater depletion potential, for a BDAC solution than for a CTAB solution at the same absolute surfactant concentration. This suggests surfactant mixtures provide a wider range of surfactant concentrations to tune and optimize NP separation.

Empirically, the critical micelle molar concentration, $C_m^*$, for a given NP and surfactant can be determined using UV−vis−NIR spectroscopy, since flocculation induces a plasmon coupling between Au NRs. Figure 4A shows the change in extinction spectra of the purified NR ($L/d = 7$) solution for increasing molar concentration of CTAB/BDAC. For an isolated NR, the longitudinal surface plasmon (LSP) and transverse surface plasmon (TSP) appear at 1063 and 505 nm, respectively. As the surfactant concentration increases above 0.2 M, the intensity of initial LSP decreases and a new peak at 791 nm appears and its intensity is increased. In addition, TSP broadens and red shifts to 530 nm. This distinctive change in LSP and TSP indicates the formation of side-by-side clusters which results in effective plasmon hybridization.[2,36] The formation of side by side clusters is consistent with geometrical arrangement providing the largest attraction depletion as well as with the microscopy of dry dispersion in parts b and f of Figure 2. The presence of an isosbestic point at 860 nm implies two species (the flocculates and isolated rods) are in dynamic equilibrium. At 0.3 M, the initial LSP completely disappears and is replaced by a peak at 791 nm. The process is reversible upon addition of Milli Q water to decrease the effective micelle molar concentration of the surfactant. The LSP and TSP shift back to the initial wavelengths (shown in Figure 4B). The surfactant concentrations of 0.2 and 0.3 M correspond to the micelle molar concentrations of 2.5 and 3.7 mM, respectively. The calculation shown in Figure 1 indicates that depletion potential between NRs of $L/d = 7$ with diameter of 10 nm becomes larger than $5k_BT$ above



DOI: 10.1021/nl100345u | *Nano Lett.* **2010,** *10,* 1433–1439

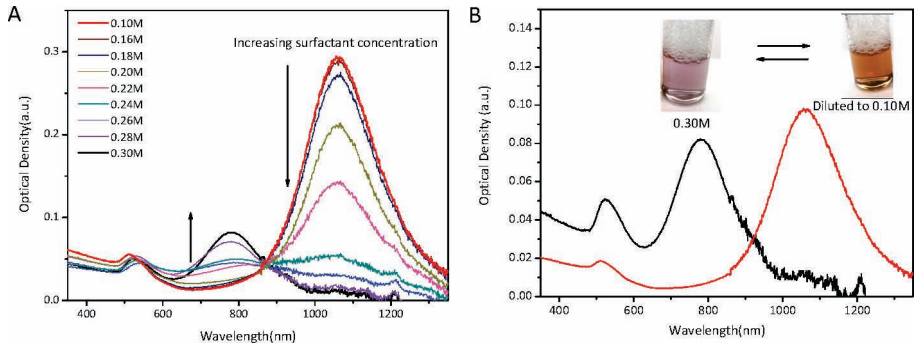


**FIGURE 4. (A) UV−vis−NIR spectra of Au NR solution (aspect ratio ~7) as a function of surfactant molar concentration of CTAB/BDAC demonstrating the formation of flocculation around the critical molar micelle concentration, $C_m$* (~3 mM, corresponding to the surfactant concentration of 0.24 M). (B) The Au NR solution at 0.3 M was diluted to 0.1 M showing reversibility of flocculation. Inset shows the color of the two solutions.**

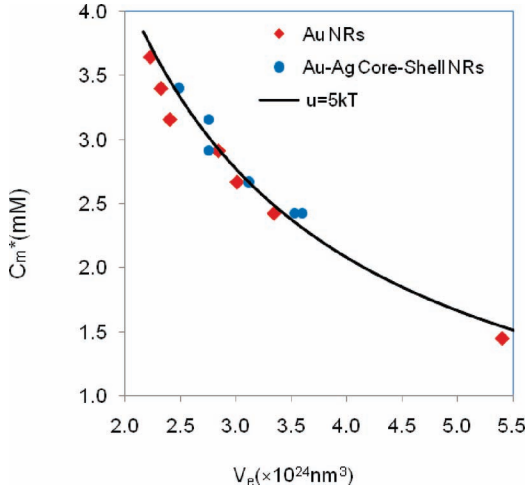


**FIGURE 5. Critical micelle molar concentration for flocculation, $C_m$* for Au NRs (red diamond shape) and Au−Ag core−shell NRs (blue circles) of increasing aspect ratio and thus excluded volume between two particles, $V_e$. Prediction of the inversely proportional relation between $C_m$* and $V_e$ from the AO model for a critical pairwise attractive potential $|U|$ of $5k_BT$ (black).**

micelle molar concentration of 3.2 mM which lies between empirically observed threshold concentrations implying that our approximation is quantitatively valid.

We also confirmed the formation of flocculation by monitoring the change of the particle size as a function of the surfactant concentration with dynamic light scattering (DLS) measurement (Figure S2). As the surfactant concentration increases, a peak due to the flocculates emerges and the size of the flocculates becomes larger (400 nm to 1200 nm) until complete sedimentation. As an example, the average size of the flocculates in 0.3 M surfactant solution (CTAB/BDAC) is 716 ± 131 nm, consistent between optical microscopy, TEM observation (Figure S3), and DLS measurement.

Figure 5 summarizes empirically estimated $C_m$* for Au NRs and Au−Ag core−shell NRs[29] of different aspect ratios that were initially separated from excess reactants and impurities and redispersed. The surfactant concentration above which the NR solution changes color was taken and used to calculate $C_m$*. As aspect ratio, and thus excluded volume increases, $C_m$* decreases. Furthermore, this relationship is independent of chemical composition (Au or Ag) of the rod surface. Most importantly, the experimental data not only exhibits the anticipated inverse proportionality between $C_m$* and $V_e$ as predicted by the AO model but quantitatively agrees with predictions based on $|U_c| \sim 5k_BT$. This is well within the expected pairwise attractive potential that would result in colloidal flocculation.

The demonstrated role of surfactant-induced depletion attraction between NPs also clarifies aspects of prior reports of separation of Au NPs of different sizes and shapes.[16,37] Considering the reported size and shape of particles and the concentration of CTAB, the calculated pair potential is consistent with separation occurring due to the significant difference in depletion interaction between NPs in solution. For example, at 0.1 M CTAB, separation of rods ($L/d = 20$, $L = 240$ nm) from spheres ($d = 50$ nm) is predicted ($5.2k_BT$ vs $2.9k_BT$, respectively),[37] where as both rods ($L/d = 15$, $L = 300$ nm) and plate (edge length = 100 nm, thickness = 20 nm) are predicted to flocculate ($6.6k_BT$ and $9.4k_BT$, respectively). These are in agreement with the reported observation.[16] For a different size of rod ($L/d = 11$, $L = 245$ nm) and plate (edge length = 70 nm), separation of rods ($5.9k_BT$) from the plates ($4.6k_BT$) is also predicted as observed.[16] The critical concentration to form flocculates (0.1 M CTAB) for these studies is lower than that discussed herein since the depletion interaction potential is greater for the larger rods and plates.

In conclusion, the concentration of surfactant micelles in a NP reaction mixture can be utilized to selectively purify the size and shape distribution of the products. As micelle molar concentration increases, NP species having larger interparticle contact area form flocculates and thus can be separated by sedimentation or centrifugation at low speed. The flocculation is reversible by subsequent reduction of surfactant concentration and independent of the NP (e.g., Au and Au−Ag core−shell NPs) or surfactant (e.g., BDAC and CTAB) composition. Most importantly, the



DOI: 10.1021/nl100345u | *Nano Lett.* **2010,** *10,* 1433–1439

critical micelle molar concentration to induce colloidal flocculation is in agreement with the AO model. These findings reinforce the hypothesis that the controlled formation of flocculates based simply on NP topology arises from surfactant micelle induced depletion potential and provides a guideline to alter processing conditions based on the relative size and concentration of NPs and surfactant micelles. Since this attractive potential depends on size and shape, and not on the chemical composition, separation approaches based on reversible depletion interactions can be applied to any mixed NP system, i.e., metallic, semiconductor, or oxide. Furthermore, the ability to quantitatively predict, experimentally measure, and reversible tune the interaction potential by surfactant composition (and temperature) implies highly refined separation based on small differences in structure, such as NR length, may be possible. Alternately, the coexistence and dynamic equilibrium between species imply controlled assembly of defect-free supercrystals akin to protein crystallites are feasible via this methodology. Thus the utilization of relatively fragile, dynamic, 1−6 nm diameter mesostructures, such as surfactant micelles or collapsed polymer chains, provides substantial opportunity to address numerous processing challenges facing wet-chemical NP technologies.

**Acknowledgment.** The authors are grateful to the Air Force Office of Scientific Research and Air Force Research Laboratory Materials & Manufacturing Directorate for financial support. We would like to thank Dr. Alexander Hexemer for guidance, setup and data collection at beamline 7.3.3 at the Advanced Light Source/LBNL.

**Supporting Information Available.** Experimental details and figures showing small-angle X-ray acattering, DLS measurments, and TEM observations. This material is available free of charge via the Internet at http://pubs.acs.org.

## REFERENCES AND NOTES

(1) Burda, C.; Chen, X.; Narayanan, R.; El-Sayed, M. A. Chemistry and Properties of Nanocrystals of Different Shapes. *Chem. Rev.* **2005**, *105* (4), 1025–1102.
(2) Cobley, C.; Skrabalak, S.; Campbell, D.; Xia, Y. Shape-Controlled Synthesis of Silver Nanoparticles for Plasmonic and Sensing Applications. *Plasmonics* **2009**, *4* (2), 171–179.
(3) Murray, C. B.; Kagan, C. R.; Bawendi, M. G. Synthesis and Characterization of Monodisperse Nanocrystals and Close-packed Nanocrystal Assemblies. *Annu. Rev. Mater. Sci.* **2000**, *30* (1), 545–610.
(4) Sohn, K.; Kim, F.; Pradel, K. C.; Wu, J.; Peng, Y.; Zhou, F.; Huang, J. Construction of Evolutionary Tree for Morphological Engineering of Nanoparticles. *ACS Nano* **2009**, *3* (8), 2191–2198.
(5) Yin, Y.; Alivisatos, A. P. Colloidal nanocrystal synthesis and the organic-inorganic interface. *Nature* **2005**, *437* (7059), 664–670.
(6) Jiang, X. C.; Brioude, A.; Pileni, M. P. Gold nanorods: Limitations on their synthesis and optical properties. *Colloids Surf., A* **2006**, *277* (1−3), 201–206.
(7) Nikhil, R. J. Gram-Scale Synthesis of Soluble, Near-Monodisperse Gold Nanorods and Other Anisotropic Nanoparticles. *Small* **2005**, *1* (8−9), 875–882.
(8) Duan, J. S.; Park, K.; MacCuspie, R. I.; Vaia, R. A.; Pachter, R. Optical Properties of Rodlike Metallic Nanostructures: Insight from Theory and Experiment. *J. Phys. Chem. C* **2009**, *113* (35), 15524–15532.
(9) Perez-Juste, J.; Pastoriza-Santos, I.; Liz-Marzan, L. M.; Mulvaney, P. Gold nanorods: Synthesis, characterization and applications. *Coord. Chem. Rev.* **2004**, *249* (17−18), 1870–1901.
(10) Xiaohua, H.; Svetlana, N.; Mostafa, A. E.-S. Gold Nanorods: From Synthesis and Properties to Biological and Biomedical Applications. *Adv. Mater.* **2009**, *21* (48), 4880–4910.
(11) Nikoobakht, B.; El-Sayed, M. A. Preparation and growth mechanism of gold nanorods (NRs) using seed-mediated growth method. *Chem. Mater.* **2003**, *15* (10), 1957–1962.
(12) Jana, N. R.; Gearheart, L.; Murphy, C. J. Wet chemical synthesis of high aspect ratio cylindrical gold nanorods. *J. Phys. Chem. B* **2001**, *105* (19), 4065–4067.
(13) Liu, F.-K.; Ko, F.-H.; Huang, P.-W.; Wu, C.-H.; Chu, T.-C. Studying the size/shape separation and optical properties of silver nanoparticles by capillary electrophoresis. *J. Chromatogr., A* **2005**, *1062* (1), 139–145.
(14) Wei, G.-T.; Liu, F.-K.; Wang, C. R. C. Shape Separation of Nanometer Gold Particles by Size-Exclusion Chromatography. *Anal. Chem.* **1999**, *71* (11), 2085–2091.
(15) Kim, F.; Song, J. H.; Yang, P. Photochemical Synthesis of Gold Nanorods. *J. Am. Chem. Soc.* **2002**, *124* (48), 14316–14317.
(16) Khanal, B. P.; Zubarev, E. R. Purification of High Aspect Ratio Gold Nanorods: Complete Removal of Platelets. *J. Am. Chem. Soc.* **2008**, *130* (38), 12634–12635.
(17) Sharma, V.; Park, K.; Srinivasarao, M. Shape separation of gold nanorods using centrifugation. *Proc. Natl. Acad. Sci. U.S.A.* **2009**, *106* (13), 4981–4985.
(18) Asakura, S.; Oosawa, F. On Interaction between Two Bodies Immersed in a Solution of Macromolecules. *J. Chem. Phys.* **1954**, *22* (7), 1255–1256.
(19) Buitenhuis, J.; Donselaar, L. N.; Buining, P. A.; Stroobants, A.; Lekkerkerker, H. N. W. Phase-Separation of Mixtures of Colloidal Boehmite Rods and Flexible Polymer. *J. Colloid Interface Sci.* **1995**, *175* (1), 46–56.
(20) Mason, T. G. Osmotically driven shape-dependent colloidal separations. *Phys. Rev. E* **2002**, *66* (6), 4.
(21) Adams, M.; Dogic, Z.; Keller, S. L.; Fraden, S. Entropically driven microphase transitions in mixtures of colloidal rods and spheres. *Nature* **1998**, *393* (6683), 349–352.
(22) Bolhuis, P. G.; Stroobants, A.; Frenkel, D.; Lekkerkerker, H. N. W. Numerical study of the phase behavior of rodlike colloids with attractive interactions. *J. Chem. Phys.* **1997**, *107* (5), 1551–1564.
(23) Yamamoto, K. R.; Alberts, B. M.; Benzinger, R.; Lawhorne, L.; Treiber, G. Rapid bacteriophage sedimentation in the presence of polyethylene glycol and its application to large-scale virus purification. *Virology* **1970**, *40* (3), 734–744.
(24) Berr, S. S. Solvent isotope effects on alkyltrimethylammonium bromide micelles as a function of alkyl chain-length. *J. Phys. Chem.* **1987**, *91* (18), 4760–4765.
(25) We provided small-angle X-ray scattering data to show the size of micelles in surfactant solution and reaction solution in the Supporting Information (Figure S1).
(26) Wang, Z. L.; Mohamed, M. B.; Link, S.; El-Sayed, M. A. Crystallographic facets and shapes of gold nanorods of different aspect ratios. *Surf. Sci.* **1999**, *440* (1−2), L809–L814.
(27) LealCalderon, F.; Gerhardi, B.; Espert, A.; Brossard, F.; Alard, V.; Tranchant, J. F.; Stora, T.; Bibette, J. Aggregation phenomena in water-in-oil emulsions. *Langmuir* **1996**, *12* (4), 872–874.
(28) Kyle, J. M. B.; Christopher, E. W.; Siowling, S.; Bartosz, A. G. Nanoscale Forces and Their Uses in Self-Assembly. *Small* **2009**, *5* (14), 1600–1630.
(29) Park, K.; Vaia, R. A. Synthesis of Complex Au/Ag Nanorods by Controlled Overgrowth. *Adv. Mater.* **2008**, *20* (20), 3882–3886.
(30) Bakshi, M.; Kaur, I. Head-group-induced structural micellar transitions in mixed cationic surfactants with identical hydrophobic tails. *Colloid Polym. Sci.* **2003**, *281* (1), 10–18.
(31) Alargova, R. G.; Kochijashky, I. I.; Zana, R. Fluorescence Study of the Aggregation Behavior of Different Surfactants in Aqueous Solutions in the Presence and in the Absence of Gas. *Langmuir* **1998**, *14* (7), 1575–1579.



DOI: 10.1021/nl100345u | *Nano Lett.* **2010,** *10,* 1433–1439

(32) Sharma, V.; Park, K.; Srinivasarao, M. Colloidal dispersion of gold nanorods: Historical background, optical properties, seed-mediated synthesis, shape separation and self-assembly. *Mater. Sci. Eng., R* **2009**, *65* (1−3), 1–38.
(33) Aswal, V. K.; Goyal, P. S. Role of different counterions and size of micelle in concentration dependence micellar structure of ionic surfactants. *Chem. Phys. Lett.* **2003**, *368* (1−2), 59–65.
(34) Link, S.; Mohamed, M. B.; El-Sayed, M. A. Simulation of the optical absorption spectra of gold nanorods as a function of their aspect ratio and the effect of the medium dielectric constant. *J. Phys. Chem. B* **1999**, *103* (16), 3073–3077.
(35) Rosen, M. J. *Surfactants and Interfacial Phenomena*, 3rd ed.; Wiley-Interscience: Hoboken, NJ, 2004.
(36) Willingham, B.; Brandl, D.; Nordlander, P. Plasmon hybridization in nanorod dimers. *Appl. Phys. B: Lasers Opt.* **2008**, *93* (1), 209–216.
(37) Jana, N. R. Nanorod shape separation using surfactant assisted self-assembly. *Chem. Commun.* **2003**, (15), 1950–1951.



DOI: 10.1021/nl100345u | *Nano Lett.* **2010,** *10,* 1433--1439